1

Preparation of 2D Materials

Yue Tang and Hua Xu

Shaanxi Normal University, Key Laboratory of Applied Surface and Colloid Chemistry of Ministry of Education, Shaanxi Key Laboratory for Advanced Energy Devices, School of Materials Science and Engineering, Xi'an 710119, P. R. China

Two-dimensional (2D) materials, an emerging new class of nanomaterials with rich structures and remarkable properties, would bring many transformative technologies and applications [1]. Since the discovery of graphene for the first time in 2004, the 2D material family has expanded dramatically to include insulators (hexagonal boron nitride [h-BN]), semiconductors (most transition metal dichalcogenides [TMDCs], black phosphorus [BP], and tellurium [Te]), semi-metals (some TMDCs and graphene), metals (transition metal carbides and nitrides [MXenes]), superconductors ($NbSe_2$), and topological insulators (Bi_2Se_3 and Bi_2Te_3) [2, 3]. The atomic thickness and dangling free surface of 2D materials, together with their superior optical, electrical, magnetism, thermal, and mechanical properties, endow them with great promise for applications in optical communication, electronics, optoelectronics, spintronics, memory, thermoelectric, and energy conversation and storage devices [4, 5].

As highlighted by the famous nanomaterial scientist Zhongfan Liu, "preparation determines the future" is an inexorable law for all materials. In the past decade, a series of preparation technologies have been developed to fabricate 2D materials for satisfying the requirements of their fundamental studies and various applications. In view of the layered structure of 2D materials, the primary preparation technologies can be divided into two major types: top-down and bottom-up approaches. In this chapter, we will introduce the recently developed preparation technologies for 2D materials, including two top-down approaches (mechanical exfoliation and liquid exfoliation) and one bottom-up approach (vapor phase growth). Here, we give more space to introduce single crystal growth, thickness control, and phase control in the vapor phase growth of 2D materials.

Two-Dimensional Materials for Nonlinear Optics: Fundamentals, Preparation Methods, and Applications, First Edition. Edited by Qiang Wang and Hao-Li Zhang.

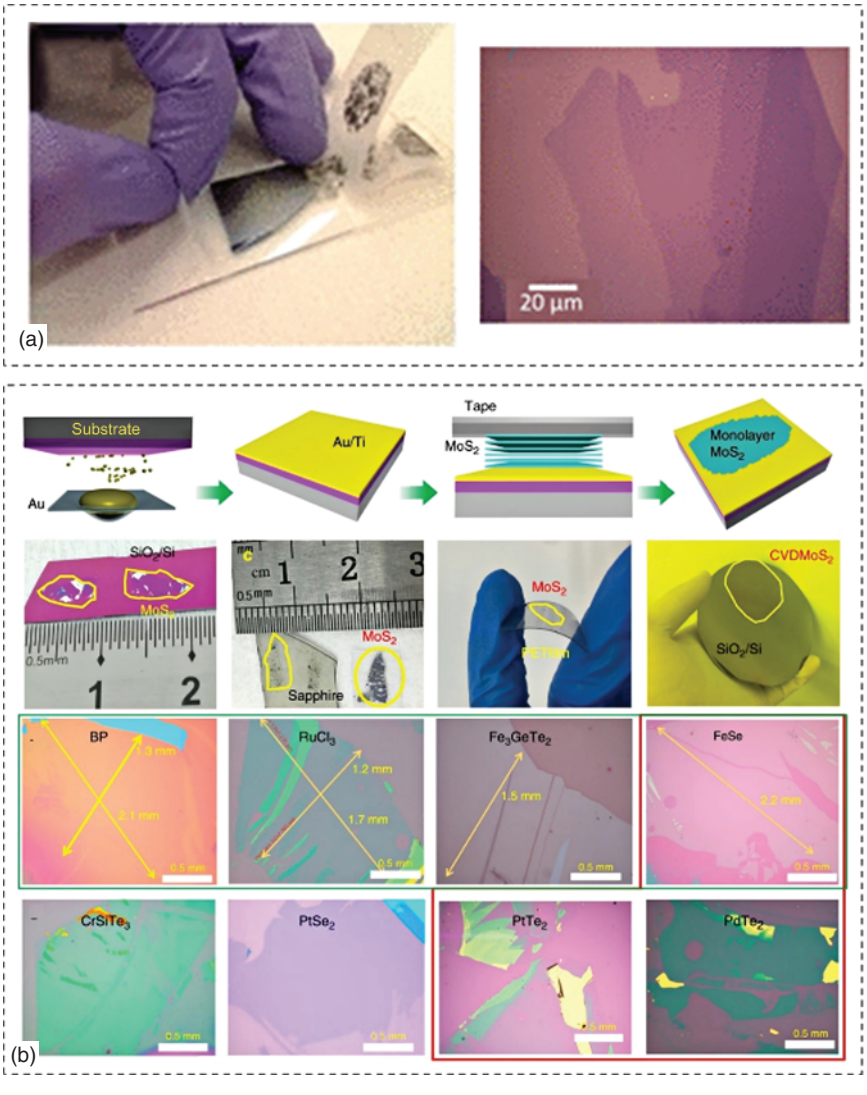

Figure 1.1 Mechanical exfoliation preparation of 2D materials. (a) Schematic diagram of mechanical cleavage process and optical micrograph of one of the graphene flakes on the SiO_2/Si substrate with different thicknesses. Source: Reproduced with permission from Yuan Huang et al. [7]/American Chemical Society. (b) Schematic diagram of the Au-assisted mechanical exfoliation process and corresponding optical microscope (OM) images of obtained vdW-layered 2D materials. Source: Yuan Huang et al. [8]/Springer Nature/CC BY 4.0.

1.1 Mechanical Exfoliation of 2D Materials

In 2004, Geim and Novosolov firstly prepared monolayer graphene by exfoliating bulk graphite using Scotch tape [6]. The schematic exfoliation method and the obtained 1-4-layer graphene are shown in Figure 1.1a [7]. Since then, mechanical cleavage, commonly referred to as the Scotch tape method and involving no

chemical reactions, is considered to be the simplest and best approach to obtain large-area, high-quality 2D materials that retain their pristine structures and properties. Until 2010, Heinz's group firstly extended the mechanical cleavage method to prepare monolayer MoS_2 and discovered the indirect to direct bandgap transition with the thickness changing from bulk to monolayer [9]. Then, A. Kis's group fabricated the field effect transistor based on the exfoliated monolayer MoS_2 and achieved room-temperature current on/off ratios of 10^8 and ultralow standby power dissipation [10]. Later, mechanical cleavage techniques were widely used to produce dozens of 2D transition metal dichalcogenides (TMDCs: WS_2, WSe_2, $MoSe_2$, ReS_2, etc.) [11]. However, with the increasing requirements on thickness and domain size of 2D materials for device fabrication and property exploration, cleavage technology pursues efficient preparation of 2D materials with large areas and high quality. Hence, many optimized mechanical cleavage techniques have been developed in recent years. For example, Huang *et al*. developed a universal Au-assisted mechanical cleavage technique, as shown in Figure 1.1b [8]. Theoretical calculation indicates that Au and many 2D materials can form quasi-covalent bonds, which are larger than van der Waals (vdW) interactions but smaller than covalent bonds. In the experiment, a thin Au layer was firstly deposited onto a substrate covered with a thin Ti or Cr adhesion layer, and a freshly cleaved bulk crystal on tape was brought into contact with the Au layer. Then the adhesive tape was placed on the outward side of the crystal, and gentle pressure was applied to establish a good crystal/Au contact. Finally, peel off the tape to remove the major portion of the crystal, leaving monolayer or few-layer flakes on the Au surface. Using this approach, they obtained large-area monolayer flakes on the Au surface, including MoS_2, FeSe, $PtSe_2$, $PtTe_2$, $PdTe_2$, and $CrSiTe_3$. Using the above exfoliation methods, a series of new 2D-layered materials have been successfully prepared, such as Fe_3GeTe_2, $MnBi_2Te_4$, CrOCl, $NbSe_2$, and $NbOCl_2$, [12–16] which exhibit superior ferromagnetic, superconduction and nonlinear optic properties. In a word, mechanical cleavage technology has been widely utilized to prepare 2D-layered materials for studying their fundamental properties.

However, the methods mentioned above are restricted to 2D-layered materials in which the interlayer interactions are dominated by weak vdW force, and thus these methods are not applicable to materials in which interlayer interactions are dominated by non-vdW force. In view of this, Zhang et al. developed a new mechanical cleavage strategy [17]. The polished metallic surface is oxidized under a controlled environment to enable the growth of hexagonal metal oxides (h-MO). These high-crystalline h-MO with layered structures, without ionic dopants or vacancies, can be easily exfoliated by stamping them onto the target substrates. This cleavage strategy was firstly applied to prepare the three-dimensional (3D) transition metal-based h-MO (TiO_2, Fe_2O_3, and Ni_2O_3), and it could be readily extended to prepare a variety of other metal oxides for exploring their novel 2D quantum properties. Most recently, Fengxia Geng's group reported a calendaring pretreatment mechanically exfoliate approach to prepare 2D materials from non-vdW structures [18]. On the basis of the traditional scotch tape method, an external mechanical force was applied to the non-vdW materials. This approach involves laterally sliding in the closely packed neighboring layers to transform the

structure from a stable to a metastable phase, weakening the interlayer binding. Using this approach, a variety of 2D materials have been prepared, including metals (Bi, Sb), semiconductors (SnO, V_2O_5, Bi_2O_2Se), and superconducting compounds (KV_3Sb_5). This method for mechanically exfoliating non-vdW materials increases the availability of 2D materials for the exploration of their physical characteristics and potential applications. To sum up, using the mechanical cleavage method can prepare most of the target 2D materials with high crystal quality, but the samples acquired via this approach also possess several problems, such as irregular morphology, uncontrollable thickness, small domain size, and low yield. Therefore, the present mechanical cleavage technology for 2D material preparation still faces great challenges, which limits its basic research to practical application. It is worth to further optimize the present cleavage methods and explore novel cleavage technologies to achieve 2D materials with controllable layers and sizes.

1.2 Liquid-Phase Exfoliation of 2D Materials

As demonstrated above, the preparation of 2D materials via mechanical exfoliation is limited by the inevitable low yield and uncontrollable thickness, domain size, and morphology. To resolve these issues, liquid-phase exfoliation (LPE) was developed to prepare 2D materials, which has the advantages of high efficiency, large scale, and better controllability [19–23]. The LPE of 2D materials can be divided into two primary approaches: direct exfoliation and chemical exfoliation [24]. Direct exfoliation methods include sonication-assisted exfoliation [SAE] and shear exfoliation. Chemical exfoliation methods include chemical intercalation and electrochemical intercalation [25, 26].

For the SAE method, layered bulk crystal was firstly dispersed in a solvent, followed by material exfoliation via ultrasonic energy and removal of the non-exfoliated material via centrifugation [27]. The dispersion is then centrifuged and purified to achieve 2D nanosheets with uniform domain size and thickness. Moreover, a shear exfoliation method has been widely used to disperse the pretreated layered crystals, which enables the production of high-quality 2D nanosheets while avoiding SAE's fragile issues. However, the exfoliation is only suitable for 2D materials with weak interlayer force, while it is difficult to effectively exfoliate 2D materials with strong interlayer coupling.

Huang et al. developed an efficient and stable three-stage sonication-assisted liquid-phase exfoliation (TS-LPE) method for mass preparation of high-structural-integrity few- and single-layer Fe_3GeTe_2 nanoflakes [28]. The three stages include slicing crystals, weakening interlayer vdW forces, and using ultrasonic cavitation (Figure 1.2a). At the first stage, ball milling is used to reduce the thickness and size of Fe_3GeTe_2 crystals. At the second stage, the shear of the solvent via stirring in *N*-methylpyrrolidone (NMP) and the shock waves caused by the collision events in the container lead to expanding layer spacing and weakening interlayer vdW forces to facilitate the subsequent shedding of the nanoflakes. The third stage is ultrasonic cavitation to facilitate the exfoliation of nanoflakes. Finally, Fe_3GeTe_2 nanoflakes

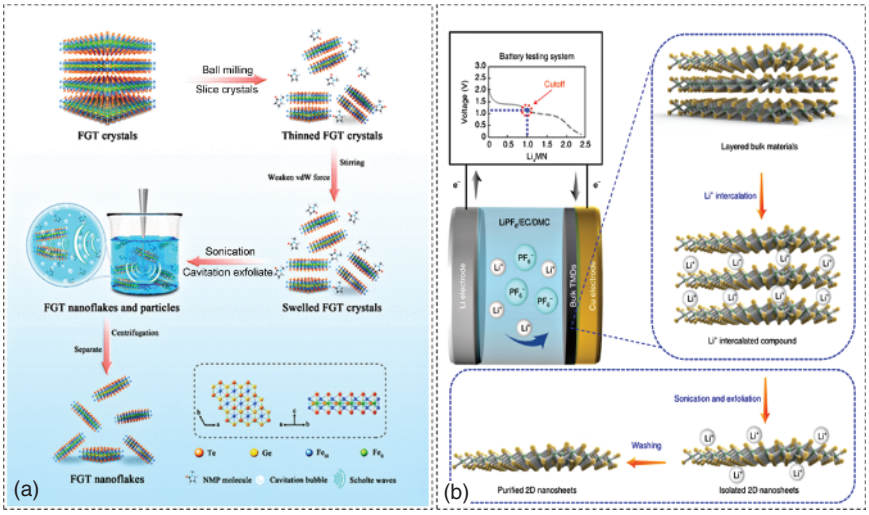

Figure 1.2 Liquid-phase exfoliation of 2D materials. (a) Schematic diagram of the TS-LPE method. Source: Reproduced with permission from Ma et al. [28]/American chemical society. (b) Schematic illustrations of the electrochemical Li^+ intercalation-based exfoliation process. Source: Reproduced with permission from Yang et al. [29]/Springer Nature.

were extracted by centrifugation. The highest yield of Fe_3GeTe_2 nanoflakes is 22.3 wt%, with single layers accounting for 6%, and a maximum of 103 μm is available. The 200 mg level of output has overcome the limitations of mechanical exfoliation and molecular beam epitaxy in economically amplificated production.

Zeng et al. developed an electrochemical lithium-ion intercalation-based exfoliation method that can be easily conducted at room temperature within 26 hours (Figure 1.2b) [29]. This exfoliation method is relatively simple and straightforward. It offers a higher degree of control under mild conditions, and thus it was widely utilized to prepare various 2D materials on a large scale. The obtained 2D nanosheets possess high crystal quality, uniform thickness, and a relatively large domain size. However, during the lithium-ion intercalation process, the insertion of each Li^+ ion involves the injection of one electron into the host crystal. Thus, the intercalation of a large number of Li^+ ions (one per formula unit in $LiMoS_2$) would lead to massive electron injection into the MoS_2 crystal, which would induce an undesired phase transition from the semiconducting 2H phase to the metallic 1T phase [30–32]. Theoretical studies suggest that this phase transition occurs only when the electron injection exceeds a certain threshold (0.29 electrons per MoS_2 formula unit) [33, 34]. A possible way of reducing electron injection into the host 2D crystal and thus preventing the undesired phase transition is to replace the small Li^+ ions (diameter $d \sim 2$ Å) with larger cations, such as quaternary ammonium ions [32]. Duan et al. developed an electrochemical exfoliation method via intercalating large-size tetramethyl ammonium bromide (THAB; $d \sim 20$ Å) molecules into the MoS_2 crystal [35]. Driven by the negative electrochemical potential, THA^+ cations were inserted into the MoS_2 layer, causing a substantial volume expansion. Then, the expanded MoS_2 crystal

was immediately sonicated in the organic solvent to disperse thin MoS_2 nanosheets within several minutes. This approach can achieve high-quality MoS_2 nanosheets on a large scale with a relatively uniform thickness that have been applied to constructing large-area thin-film electronic devices, and this method has been extended to prepare other 2D TMDs [20, 36].

To sum up, the LPE method can prepare large-scale 2D materials with monolayer and few-layer, but it still needs to improve the controllability of thickness and morphology. In addition, high-power ultrasonic energy, organic solvents, or chemical intercalators inevitably degenerate the intrinsic structure and properties of 2D materials, which hinders their high-performance optical and electronic applications. Hence, the 2D materials prepared by LPE methods are favorable to some particular fields, such as supercapacitors, lithium-ion batteries, catalysis, printer ink, and composite materials.

1.3 Chemical Vapor Deposition Growth of 2D Materials

Comparing with the above top-down methods, bottom-up synthesis by chemical vapor deposition (CVD) proves to be an effective method to grow large-scale 2D materials with controllable domain size, morphology, thickness, and electronic-grade quality, which shows great potential for fabricating high-performance optical, electronic, and optoelectronic devices for commercial applications. The CVD method used to synthesize 2D materials refers to the gas-vapor growth of material on a substrate within the tube furnace system (Figure 1.3a) [37, 41]. To be specific, two or more precursors are introduced into the high-temperature reaction zone in quartz tube by carrier gas for chemical reaction, nucleation, growth, and final formation of 2D flakes or continuous films on the substrate.

In the past decades, CVD has been widely used in the preparation of various 2D materials, such as elemental graphene and BP, binary h-BN, TMDs (MoS_2, WSe_2, $MoTe_2$, VS_2, TiS_2, $ReSe_2$, etc.), ternary chalcogenides, and their alloys and heterostructures [42–47]. Take the CVD growth of MoS_2 as an example, Van der Zande et al. synthesized monolayer MoS_2 nanosheets with uniform triangle morphology by using CVD growth with sulfur (S) powder and molybdenum trioxide (MoO_3) as precursors [48]. The obtained MoS_2 possesses high-quality, uniform monolayer and large grain size up to 120 μm, which enables comparable electrical and photoelectric properties with those of mechanically exfoliated MoS_2.

During the process of 2D material growth, many factors affect the quality and properties of the product, such as precursor, substrate, growth temperature, carrier gas flow, and additives [49–51]. Thus, great efforts have been made to optimize the CVD growth method to achieve the preparation of large-area, high quality, homogeneous-thickness 2D materials [49]. For instance, to achieve a stable and continuous supply of Mo source, electrochemically oxidized arched Mo foil was utilized as the precursor instead of the traditional powder, and the growth of MoS_2 with controllable thickness was realized (Figure 1.3b) [38]. In addition, researchers have confirmed that the addition of synergistic additives can modulate the growth chemistry of 2D materials, facilitate the growth rate, and adjust the morphology and

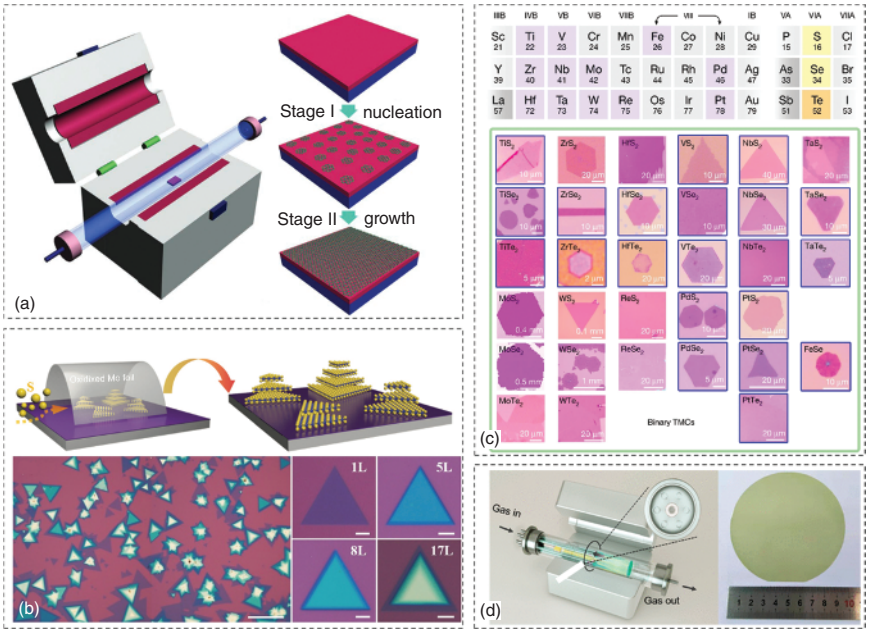

Figure 1.3 CVD growth of 2D materials. (a) Schematic diagram of the CVD setup and the main growth process [37]. (b) Schematics of the CVD growth of MoS_2 using arched oxidized Mo foil as precursor and optical images of the growth products with varied thickness. Source: Reproduced with permission from Jingying Zheng et al. [38]/John Wiley & Sons. (c) The transition metals and chalcogens used for molten salt-assisted CVD growth and optical images of the different atomically thin TMCs. Source: Reproduced with permission from Jiadong Zhou et al. [39]/Springer Nature. (d) Schematic diagram of the multi-source CVD setup and photograph of a monolayer MoS_2 film at a 4 in. wafer scale. Source: Reproduced with permission from Qinqin Wang et al. [40]/American Chemical Society.

structure. For many 2D TMDs, the high melting point of metal precursors leads to a challenge for low-temperature growth through CVD. In view of this, Zhou et al. developed a molten salt-assisted CVD method and demonstrated that salt decreases the melting point of the reactants and increases the overall reaction rate, which is favorable for highly efficiently achieving various 2D TMDs (Figure 1.3c) [39]. Moreover, by introducing fluorine into the growth system, Liu et al. demonstrated that the growth rate of graphene, h-BN, and WS_2 could be greatly accelerated, which is beneficial for growing large domain-size 2D materials [52].

Owing to the inherent difficulty in controlling the concentration of solid precursors during the entire growth time, it remains a challenge to prepare large-area monolayer films with spatial homogeneity and structural continuity. Kang et al. adopted a metal-organic chemical vapor deposition (MOCVD) technique, with $Mo(CO)_6$, $W(CO)_6$, $(C_2H_5)_2S$, and H_2 as independent gas-phase precursors, to grow large-area and uniform 2D TMD films [53]. They demonstrated that maintaining a low partial pressure at the Mo source by controlling the partial pressure is the key to the layer-by-layer growth and the formation of a wafer-scale TMDs film. Furthermore, since the configuration of the CVD instrument may play an important role in 2D material growth, many studies have also focused on the optimization of

the CVD system [54, 55]. For example, Wang et al. designed a multisource supply tube in the traditional CVD setup to ensure a sufficient and uniform precursor supply, and the c-sapphire substrate was vertically placed in the growth chamber to avoid precursor concentration inhomogeneity along the gas flow direction. Using this CVD setup, they successfully obtained wafer-scale MoS_2 films with domain sizes up to 180 μm (Figure 1.3d) [40].

Although CVD-growth of 2D materials has made great progress in the past decades, the controllable growth of 2D materials still faces great challenges in thickness control, wafer-scale single-crystal preparation, and phase modulation. Moreover, there is great development space to combine various 2D materials with distinct structures and properties to build 2D alloys and heterostructures to satisfy their various applications. The specific CVD growth strategies for the controllable preparation of 2D materials, including wafer-scale single crystal, thickness control, and phase modulation, will be introduced in detail in the following sections.

1.4 CVD Growth of Wafer-Scale Single Crystal 2D Materials

In most of the present works, amorphous SiO_2/Si was primarily used as the substrate in CVD growth of 2D materials, which results in the random orientation of 2D grains [48]. Thus, CVD-grown 2D films are usually polycrystalline with many grain boundaries, which seriously deteriorates their optical, electrical, mechanical, chemical, stability, etc. To improve these properties, it is highly desired to prepare 2D films with uniform thickness, high crystallinity, defect-free, and limited grain boundaries, especially wafer-scale single crystal 2D films [56]. Substrate-guided epitaxial growth is widely utilized to achieve these 2D films. The idea is based on the effective control of the orientation of 2D materials grown on a substrate, where the grains merge seamlessly with the same (or small misorientation) angle, which is considered to be an essential way to decrease or eliminate the grain boundaries [57].

Most 2D TMDs have a threefold symmetry structure, thus the lattice-induced epitaxial can be used to achieve wafer-scale 2D films. So, the c-plane sapphire, which has the same symmetry and compatible lattice constant with TMDs, has been widely used as a substrate to align the TMDs [40, 58]. However, the epitaxial relationship indicates that the $[11\bar{2}0]$ direction of the c-plane sapphire is perpendicular to the zig-zag edge of TMD domains, which equalizes the two antiparallel domains and prevents the growth of single crystals. To solve the above problem, Wang et al. designed a c-plane sapphire wafer with a major miscut angle toward the A axis (defined as C/A), which produced surface steps along $< 10\bar{1}0 >$ direction for unidirectionally aligning MoS_2, as shown in Figure 1.4a [59]. In principle, a good epitaxial relationship between MoS_2 and c-plane sapphire is formed (Figure 1.4b) when the armchair and zigzag directions of MoS_2 are parallel to $< 11\bar{2}0 >$ and $< 10\bar{1}0 >$ of Al_2O_3, respectively. An OM image of as-grown triangular MoS_2 domains on c-plane sapphire shows an obvious unidirectional alignment. Second harmonic generation (SHG) mapping of two adjacent MoS_2 grains (Figure 1.4d)

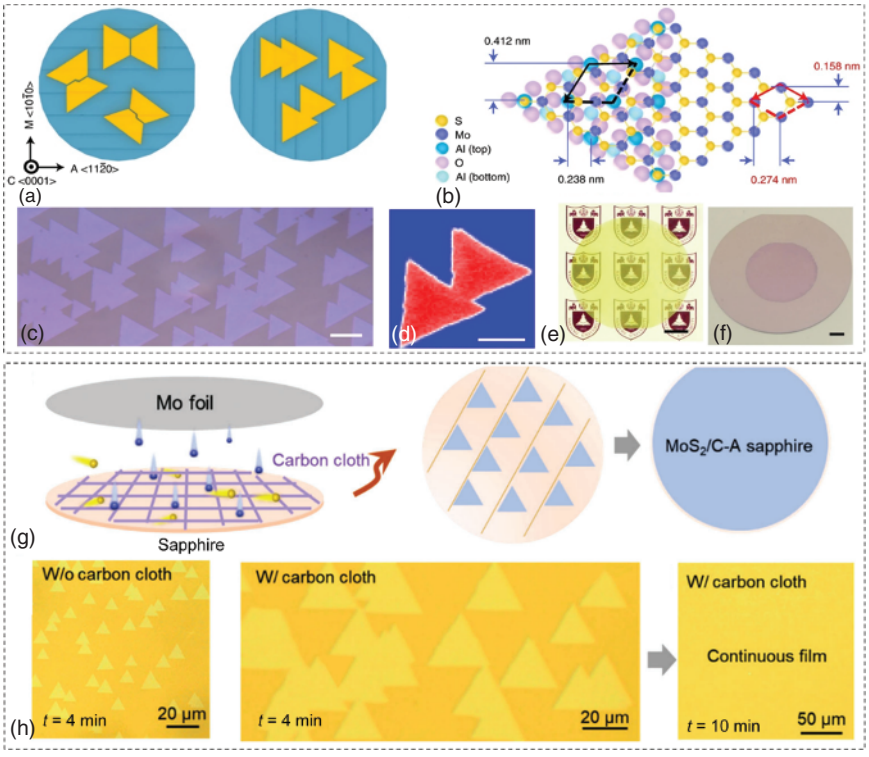

Figure 1.4 CVD growth of wafer-scale single-crystal 2D materials. (a) Schematically show the epitaxial relationship between MoS_2 grain and c-plane sapphire with different step orientations. Source: Taotao Li et al. [59]/Reproduced with permission of Springer Nature. (b) The epitaxial relationship of MoS_2 on c-plane sapphire in atomic scale. Source: Taotao Li et al. [59]/Reproduced with permission of Springer Nature. (c) Unidirectional alignment of MoS_2 domains on a C/A sapphire (0001) substrate. Source: Taotao Li et al. [59]/Reproduced with permission of Springer Nature. (d) Polarized SHG mapping of two merging MoS_2 domains on the C/A sapphire (0001) substrate. Source: Reproduced with permission from Taotao Li et al. [59]/Springer Nature. (e, f) Photographs of 2-inch monolayer MoS_2 single crystal on C/A sapphire and SiO_2/Si substrates. Source: Taotao Li et al. [59]/Reproduced with permission of Springer Nature. (g) Schematic illustration of the carbon-cloth shield over sapphire template-assisted growth of monolayer MoS_2 single crystal. Source: Pengfei Yang [60]/Reproduced with permission from John Wiley & Sons. (h) Epitaxial growth of 2-inch uniform monolayer MoS_2 single crystal on sapphire. Source: Reproduced with permission from Pengfei Yang [60]/John Wiley & Sons.

shows uniform intensity, suggesting the same grain orientations without an obvious grain boundary. By extending the growth time, they obtained wafer-scale (2-inch) monolayer MoS_2 films that can be easily transferred to arbitrary substrates (Figure 1.4e,f). Zhang et al. reported the epitaxial growth of wafer-scale MoS_2 single crystal on sapphire with Mo foil and S powder as precursors [60]. The carbon cloth layer placed between Mo film and sapphire substrate ensures the homogenous and continuous Mo supply (Figure 1.4g), which enables uniform nucleation and growth of monolayer MoS_2 film. In addition, the commensurability between MoS_2 lattice

and sapphire lattice and the guiding effect of sapphire step edges are proposed to direct the unidirectionally aligned growth of monolayer MoS_2 single crystals. The aligned seed crystal can be seamlessly stitched to a continuous single crystal film by increasing growth time (Figure 1.4h). Moreover, Xu et al. reported an epitaxial growth of highly aligned MoS_2 grains on a twofold symmetry a-plane sapphire substrate [61]. The obtained MoS_2 grains have an unusual rectangle shape with perfect orientation alignment along the $< 1\bar{1}00 >$ direction of a-plane sapphire. They found that high temperature is beneficial to the MoS_2 seeds rotation to a favorable orientation, which is beneficial for the unidirectional alignment of MoS_2.

Many efforts have been devoted to grow wafer-scale non-centrosymmetric 2D materials by aligning unidirectional grains on single-crystal substrates [62–64]. The aligned domains can be seamlessly stitched, and then the 2D film is formed. Liu et al. reported the growth of a wafer-scale single crystal h-BN monolayer on a vicinal Cu (110) substrate [64]. The Cu (110) vicinal surface, on which the presence of metal steps uniformly along the <211> direction leads to a C_1 symmetry, is critical to prepare the unidirectional arrangement of the h-BN monolayer. The step edges reduced the symmetry of the substrate, broke the energetical degeneracy of the antiparallel domains, and aligned the domain orientation. The h-BN single crystal grains are nucleated near the step edges, with one edge of the grains tightly attached to the upward side of the step edge during the growth process, and the grains propagate rapidly on the plateau between neighboring step edges. Once one of its edges reached a neighboring step edge in the downward direction, the propagation of the edge was temporarily arrested, and finally spliced into a continuously single-crystalline 2D film. Using this method, the unidirectional alignment of h-BN grains can be achieved on a large scale.

Beside the substrate-guided epitaxial growth strategy, a seed-induced epitaxial growth strategy was also developed for controllable fabrication of wafer-scale single crystal 2D TMDs films. For example, Ye et al. reported the synthesis of a large-area 2H-$MoTe_2$ single crystal via solid-to-solid transition and recrystallization process, where a piece of 2H-$MoTe_2$ as a seed crystal was implanted into the 1T′-$MoTe_2$ film to trigger the in-plane 2D-epitaxy growth [65]. The resulting single-crystalline film completely covered a 2.5-cm wafer with excellent uniformity.

1.5 Thickness Control in CVD Growth of 2D Materials

As we all know, the properties of 2D materials are closely related to their layer numbers [9, 38]. For example, compared with the single layer, the bilayer TMDs have good electrostatic control, a smaller band gap, and higher mobility, which will improve the energy-delay product of the transistor [66–69]. Hence, the preparation of high-quality 2D films with controllable layers is another important project in this field. In the traditional CVD growth process, the continuous flow of carried gas in the same direction leads to the random growth of many small triangular grains (the second layer) on the surface of monolayer crystal (the first layer), which makes the controllable growth of uniform multiple TMD layers much more

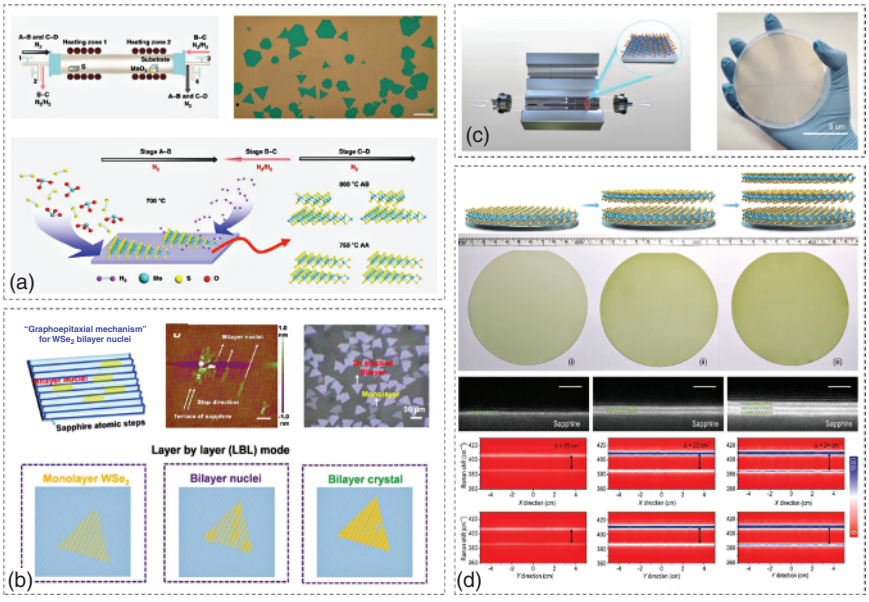

Figure 1.5 Thickness control for CVD growth of 2D materials. (a) Schematic diagram of reverse-flow CVD process for growing bilayer MoS_2 and corresponding OM image of obtained bilayer MoS_2. Source: Xiumei Zhang [71]/Springer Nature/CC BY 4.0. (b) Schematic diagram of the bilayer WSe_2 epitaxy growth process on c-plane sapphire and the corresponding AFM and OM images. Source: Reproduced with permission from Ali Han et al. [72]/Reproduced with permission from Royal Society of Chemistry. (c) Diagram of the CVD growth of wafer-scale (4-inch) $MoSe_2$ in three-temperature-zone tube furnace. Source: Jiawei Li et al. [73]/John Wiley & Sons/CC BY 4.0. (d) Schematic diagram of layer-by-layer epitaxy of multilayer wafer MoS_2 and corresponding photographs, STEM images (cross-section), and Raman spectra line mapping images of the wafers. Source: Qinqin Wang et al. [74]/Oxford University Press/CC BY 4.0.

difficult [70]. Ostrikov et al. developed a reverse-flow CVD growth strategy to prepare the uniform bilayer MoS_2 [71]. The detailed growth produced is shown in Figure 1.5a. Different from the traditional CVD method with constant gas flow direction during the entire growth process, here they introduced a reverse airflow in the variable temperature section (b–c section). This reverse gas flow reduces uncontrolled nucleation and promotes uniform epitaxy of the second monolayer from the active nucleation center on the first monolayer. This approach enables high-quality, uniform bilayer MoS_2 crystals with high yield, controllability, and reliability, and it provides a possible route for the subsequent large-scale growth of 2D materials with controllable layers. Wu et al. successfully grew a controllable three-layer MoS_2 with high mobility and large single crystals on a sodium-lime glass substrate by using a CVD strategy [75]. In addition, Zhang et al. used a similar reverse-flow CVD growth strategy to inhibit the uncontrolled nucleation and thus achieved the highly robust epitaxial growth of various 2D heterogeneous structures and superlattices [51]. Li et al. reported the controlled growth of 2H-stacked bilayer

WSe_2 by CVD growth on a c-plane sapphire substrate with atomic steps, as shown in Figure 1.5b [72]. They demonstrate that the nuclei growth of bilayer WSe_2 slides along the pronounced atomic steps induced by WSe_2 crystals atop, resembling the graphoepitaxy mechanism.

Though great progress has been made in the growth of multilayer TMD grains, achieving wafer-scale multilayer TMD films remains a big challenge. Wang et al. report the step-induced uniform nucleation (>99%) of bilayer MoS_2 on c-plane sapphire [76]. According to DFT calculations, a bilayer nucleation with aligned edges is required before merging to obtain a uniform bilayer TMDs film, and the interfacial formation energy of bilayer MoS_2 markedly decreases with step height. In an experiment, they explored the atomic terrace height on c-plane sapphire to enable an edge-nucleation mechanism and the coalescence of MoS_2 domains into continuous, centimeter-scale films. Moreover, Zhang's group devotes a great effect on the growth of wafer-scale multilayer 2D TMDs. They firstly developed a multi-channel source-supply CVD strategy to grow wafer-scale (4-inch) single-layer $MoSe_2$ film in a three-temperature zone tubular furnace [73]. In this work, they placed the sources in different temperature zones, with the sapphire substrate placed vertically in the third temperature zone. Especially, three small quartz tubes in the growth chamber act as containers for MoO_3, each capable of independently transporting carrier gas. This multi-channel design provides an even and continuous precursor supply, allowing uniform nucleation of $MoSe_2$ across the entire wafer with high nucleation density and the ability to grow wafer-scale monolayers in a short period of time. This work provides an important foundation for the subsequent wafer-scale growth of multilayer TMD films. Zhang et al. report the layer-by-layer epitaxy process growth method for preparing high-quality 4-inch multilayer MoS_2 wafers on sapphire substrate [74]. Firstly, monolayer MoS_2 is prepared by domain-domain coalescence in a multi-channel oxygen-enhanced CVD system. Then, additional epitaxial layers are grown on top of the first layer using the same technique to control the number of layers, resulting in multilayers of MoS_2 with clean, sharp interface atoms. The layer-by-layer epitaxial growth process enables a well-defined stack sequence with precise control over the number of layers, up to six. Furthermore, recent studies have demonstrated the successful synthesis of high-quality wafer-scale multilayer 2D films such as graphene and h-BN by reasonably designing the CVD growth conditions and processes [77–79]. Above progresses on thickness-controllable preparation of 2D materials provides the material foundation for exploring their thickness-dependent properties and device applications. With the development of new CVD technology, it is believed that the thickness-controllable preparation of many other 2D materials will be realized in the near future.

1.6 Phase Control in CVD Growth of 2D Materials

The phase multiplicity of 2D materials is pivotal for exploring their novel physical and chemical properties [80]. For example, most 2D TMDs (MoS_2, WS_2, WSe_2, etc.)

possess a stable 2H phase and a metastable 1T and 1T′ phase, which exhibit semiconducting and metallic properties, respectively [5]. Moreover, researchers found that the semiconducting 2H $MoTe_2$ might be commendable in thermoelectricity [81], and the metallic 1T′ $MoTe_2$ has extremely large magnetoresistance and quantum spin Hall effect [82, 83]. Interestingly, the hexagonal and tetragonal FeTe nanosheets were demonstrated to possess ferromagnetism and antiferromagnetism, respectively [84].

Phase engineering of 2D materials during the CVD growth process is much important to explore their various properties and device applications. One of the important approaches for phase engineering is to realize the phase transformation of existing 2D materials in a CVD system. Ye et al. reported a route for synthesizing wafer-scale single-crystalline 2H $MoTe_2$ by in-plane epitaxial tellurizing, which was triggered by a deliberately implanted single seed crystal [65]. Hu et al. realized a large-scale selective growth of the 1T′/2H/1T′ $MoTe_2$ multiphase structure, with the 1T′ and 2H phases seamlessly stitched [85]. The various phase transformation methods not only provide convenient and effective approaches readily applicable in many applications but also play critical roles in understanding the fundamentals of how crystal phases impact their properties.

Compared with the phase transformation method, the direct synthesis of 2D materials with distinct phase structures is more favorable to achieve a high-purity phase structure. CVD growth has great potential in the phase-controllable synthesis of 2D materials because of its diverse growth parameters (temperature, precursor, carrier gas, composition, etc.) [86]. For example, Jiao et al. reported the phase-selective growth of 1T′ and 2H MoS_2 monolayers and 1T′/2H heterophase bilayers using a potassium (K)-assisted CVD method [87]. This was realized by using K_2MoS_4 as a precursor and tuning the concentration of K in the growth products to invert the stability of the 1T′ and 2H phases. In Figure 1.6a, Xu et al. developed a facile CVD method to synthesize high-quality $Mo_xRe_{1-x}S_2$ alloys with tunable composition and phase structure [88]. The 1T′ phase $Mo_xRe_{1-x}S_2$ alloys were obtained for x in the range of 0–0.25, while the 2H phase $Mo_xRe_{1-x}S_2$ alloys were achieved for x in the range of 0.75–1. Liu et al. selectively synthesized the hexagonal phase and the tetragonal phase FeTe nanosheets on SiO_2/Si by controlling the growth temperature during the CVD process (Figure 1.6b) [84]. The phase-controllable growth of FeTe originates from the formation energy difference between the hexagonal and tetragonal phases, and maintaining a relatively high temperature is essential for obtaining the thermodynamically stable hexagonal phase, while a low temperature is favorable to the tetragonal phase. Most recently, Zhao et al. synthesized both pure β and β′ In_2Se_3 by means of controlling whether to add InSe into the In_2O_3 precursor [89]. Using DFT calculations and in situ TEM experiments, they confirm that the Se deficiency triggers the $\beta \rightarrow \beta'$ phase transition, which effectively explains the seeding effect of InSe additive in CVD precursors for the β′-phase growth. The above results demonstrate the feasibility of CVD synthesis of large-area, highly crystalline 2D materials with controllable phase structures, which is highly desirable for their promising wide applications.

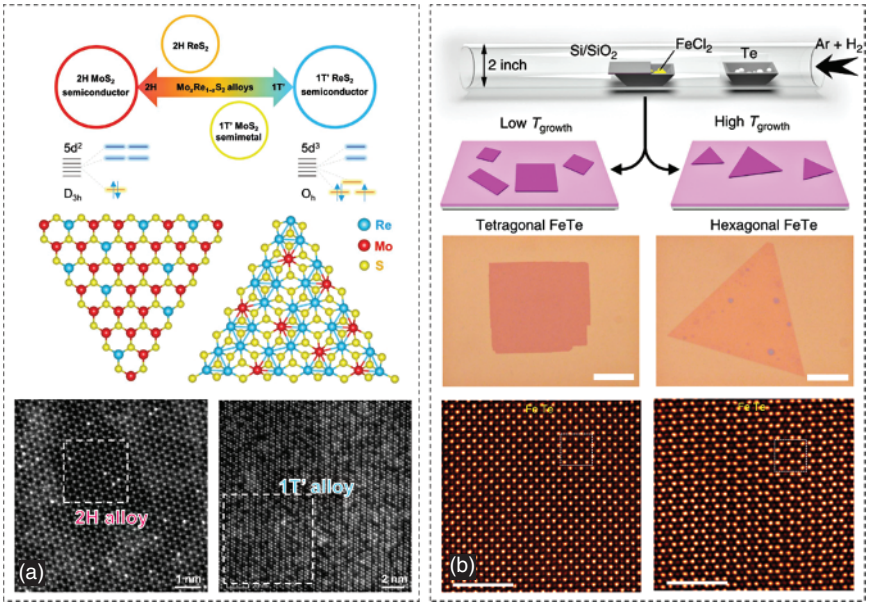

Figure 1.6 Phase-tunable synthesis of 2D materials. (a) Schematic illustration of the structure, phase, and energy band engineering of $Mo_xRe_{1-x}S_2$ alloys, the atomic structure of 2H and 1T′ $Mo_xRe_{1-x}S_2$ alloys, and the ADF-STEM images of 1T′ and 2H $Mo_xRe_{1-x}S_2$ alloys. Source: Reproduced with permission from Qixin Deng et al. [88]/John Wiley & Sons. (b) Schematic view for the temperature-modulated phase selective growth process of FeTe, the OM images (scale bar: 20 μm) and atomic-resolution STEM-ADF images (scale bar: 5 nm) of tetragonal and hexagonal FeTe nanosheets. Source: Lixing Kang et al. [84]/Springer Nature/CC BY 4.0.

1.7 Summary and Prospect

Over the past two decades, the preparation of 2D materials has made tremendous progress, which greatly promotes the fast development of the 2D field. To realize the high-efficiency synthesis of 2D materials with controllable thickness, domain size, crystal quality, and phase structures, researchers have developed a series of preparation approaches, including mechanical exfoliation, LPE, and CVD. The various preparation methods possess their own advantages and disadvantages, and thus the obtained 2D materials exhibit distinct features that fulfill the requirements of their diverse applications. In brief, the mechanical cleavage method can prepare most of the target 2D materials with high crystal quality, but the samples acquired via this approach also possess several problems, such as irregular morphology, uncontrollable thickness, small domain size, and low yield. The corresponding 2D materials are primarily used to explore their fundamental properties. LPE is suitable for large-scale production at a low cost, but precise control of size and layer number with preservation of pristine quality is still highly challenging. The obtained 2D materials exhibit prominent superiorities in some special applications, such as lithium-ion batteries, catalysis, printer ink, and composite materials. Bottom-up

synthesis via CVD growth has emerged as a versatile and scalable approach enabling precise control over the thickness, morphology, crystallinity, and phase structure, which provides significant opportunities for exploring their fundamental physics and device applications.

References

1 Akinwande, D., Huyghebaert, C., Wang, C.-H. et al. (2019). Graphene and two-dimensional materials for silicon technology. *Nature* 573 (7775): 507–518.

2 Giri, A., Park, G., and Jeong, U. (2023). Layer-structured anisotropic metal chalcogenides: recent advances in synthesis, modulation, and applications. *Chemical Reviews* 123: 3329–3442.

3 Novoselov, K.S., Mishchenko, A., Carvalho, A., and Castro Neto, A.H. (2016). 2D materials and van der Waals heterostructures. *Science* 353 (6298): aac9439.

4 Polyushkin, D.K., Wachter, S., Mennel, L. et al. (2020). Analogue two-dimensional semiconductor electronics. *Nature Electronics* 3 (8): 486–491.

5 Chhowalla, M., Shin, H.S., Eda, G. et al. (2013). The chemistry of two-dimensional layered transition metal dichalcogenide nanosheets. *Nature Chemistry* 5 (4): 263–275.

6 Novoselov, K.S., Geim, A.K., Morozov, S.V. et al. (2004). Electric field effect in atomically thin carbon films. *Science* 306 (5696): 666–669.

7 Huang, Y., Sutter, E., Shi, N.N. et al. (2015). Reliable exfoliation of large-area high-quality flakes of graphene and other two-dimensional materials. *ACS Nano* 9 (11): 10612–10620.

8 Huang, Y., Pan, Y.-H., Yang, R. et al. (2020). Universal mechanical exfoliation of large-area 2D crystals. *Nature Communications* 11 (1): 2453.

9 Mak, K.F., Lee, C., Hone, J. et al. (2010). Atomically thin MoS_2: a new direct-gap semiconductor. *Physical Review Letters* 105 (13): 136805.

10 Radisavljevic, B., Radenovic, A., Brivio, J. et al. (2011). Single-layer MoS_2 transistors. *Nature Nanotechnology* 6 (3): 147–150.

11 Xin-Yu, H., Xu, H., Hui, C. et al. (2022). New progress and prospects of mechanical exfoliation technology of two-dimensional materials. *Acta Physica Sinica* 71 (10): 108201.

12 Guo, Q.B., Qi, X.-Z., Zhang, L.S. et al. (2023). Ultrathin quantum light source with van der Waals $NbOCl_2$ crystal. *Nature* 613 (7942): 53–59.

13 Deng, Y.J., Yu, Y.J., Song, Y.C. et al. (2018). Gate-tunable room-temperature ferromagnetism in two-dimensional Fe_3GeTe_2. *Nature* 563 (7729): 94–99.

14 Xu, X.L., Yang, S.Q., Wang, H. et al. (2022). Ferromagnetic-antiferromagnetic coexisting ground state and exchange bias effects in $MnBi_4Te_7$ and $MnBi_6Te_{10}$. *Nature Communications* 13 (1): 7646.

15 Wang, M.X., Zhang, J., Wang, Z.P. et al. (2019). Broadband CrOCl saturable absorber with a spectral region extension to 10.6 μm. *Advanced Optical Materials* 8 (2): 1901446.

16 Xi, X.X., Wang, Z.F., Zhao, W.W. et al. (2015). Ising pairing in superconducting $NbSe_2$ atomic layers. *Nature Physics* 12 (2): 139–143.

17 Zhang, B.Y., Xu, K., Yao, Q. et al. (2021). Hexagonal metal oxide monolayers derived from the metal–gas interface. *Nature Materials* 20 (8): 1073–1078.

18 Jiang, K., Ji, J.P., Gong, W.B. et al. (2022). Mechanical cleavage of non-van der Waals structures towards two-dimensional crystals. *Nature Synthesis* 2 (1): 58–66.

19 Pinilla, S., Coelho, J., Li, K. et al. (2022). Two-dimensional material inks. *Nature Reviews Materials* 7 (9): 717–735.

20 Coleman, J.N., Lotya, M., O'Neill, A. et al. (2011). Two-dimensional nanosheets produced by liquid exfoliation of layered materials. *Science* 331 (6017): 568–571.

21 Li, H.L., Jing, L., Liu, W.W. et al. (2018). Scalable production of few-layer boron sheets by liquid-phase exfoliation and their superior supercapacitive performance. *ACS Nano* 12 (2): 1262–1272.

22 Kaur, H. and Coleman, J.N. (2022). Liquid-phase exfoliation of nonlayered non-Van-Der-Waals crystals into nanoplatelets. *Advanced Materials* 34 (35): 2202164.

23 Cullen, P.L., Cox, K.M., Bin Subhan, M.K. et al. (2017). Ionic solutions of two-dimensional materials. *Nature Chemistry* 9 (3): 244–249.

24 Grayfer, E.D., Kozlova, M.N., and Fedorov, V.E. (2017). Colloidal 2D nanosheets of MoS_2 and other transition metal dichalcogenides through liquid-phase exfoliation. *Advances in Colloid and Interface Science* 245: 40–61.

25 Eda, G., Yamaguchi, H., Voiry, D. et al. (2011). Photoluminescence from chemically exfoliated MoS_2. *Nano Letters* 11 (12): 5111–5116.

26 Lam, D., Lebedev, D., Kuo, L. et al. (2022). Liquid-phase exfoliation of magnetically and optoelectronically active ruthenium trichloride nanosheets. *ACS Nano* 16 (7): 11315–11324.

27 Huo, C.X., Yan, Z., Song, X.F., and Zeng, H.B. (2015). 2D materials via liquid exfoliation: a review on fabrication and applications. *Scientific Bulletin* 60 (23): 1994–2008.

28 Ma, S., Li, G., Li, Z. et al. (2022). 2D Magnetic semiconductor Fe(3)GeTe(2) with few and single layers with a greatly enhanced intrinsic exchange bias by liquid-phase exfoliation. *ACS Nano* 16 (11): 19439–19450.

29 Yang, R., Mei, L., Zhang, Q. et al. (2022). High-yield production of mono- or few-layer transition metal dichalcogenide nanosheets by an electrochemical lithium ion intercalation-based exfoliation method. *Nature Protocols* 17 (2): 358–377.

30 Zeng, Z.Y., Yin, Z.Y., Huang, X. et al. (2011). Single-layer semiconducting nanosheets: high-yield preparation and device fabrication. *Angewandte Chemie, International Edition* 123 (47): 11289–11293.

31 Kappera, R., Voiry, D., Yalcin, S.E. et al. (2014). Phase-engineered low-resistance contacts for ultrathin MoS_2 transistors. *Nature Materials* 13 (12): 1128–1134.

32 Li, J., Song, P., Zhao, J.P. et al. (2021). Printable two-dimensional superconducting monolayers. *Nature Materials* 20 (2): 181–187.

33 Li, Y., Duerloo, K.A., Wauson, K., and Reed, E.J. (2016). Structural semiconductor-to-semimetal phase transition in two-dimensional materials induced by electrostatic gating. *Nature Communications* 7: 10671.

34 Wang, Y., Xiao, J., Zhu, H.Y. et al. (2017). Structural phase transition in monolayer $MoTe_2$ driven by electrostatic doping. *Nature* 550 (7677): 487–491.

35 Lin, Z.Y., Liu, Y., Halim, U. et al. (2018). Solution-processable 2D semiconductors for high-performance large-area electronics. *Nature* 562 (7726): 254–258.

36 Ciesielski, A. and Samori, P. (2016). Supramolecular approaches to graphene: from self-assembly to molecule-assisted liquid-phase exfoliation. *Advanced Materials* 28 (29): 1505371.

37 Chen, J.Y., Guo, Y.L., Wen, Y.G. et al. (2013). Two-stage metal-catalyst-free growth of high-quality polycrystalline graphene films on silicon nitride substrates. *Advanced Materials* 25 (7): 992–997.

38 Zheng, J.Y., Yan, X.X., Lu, Z.X. et al. (2017). High-mobility multilayered MoS_2 flakes with low contact resistance grown by chemical vapor deposition. *Advanced Materials* 29 (13): 1604540.

39 Zhou, J.D., Lin, J.H., Huang, X.W. et al. (2018). A library of atomically thin metal chalcogenides. *Nature* 556 (7701): 355–359.

40 Wang, Q., Li, N., Tang, J. et al. (2020). Wafer-scale highly oriented monolayer MoS_2 with large domain sizes. *Nano Letters* 20 (10): 7193–7199.

41 Sun, L.Z., Yuan, G.W., Gao, L.B. et al. (2021). Chemical vapour deposition. *Nature Reviews Methods Primers* 1 (1): 5.

42 Cai, Z.Y., Liu, B.L., Zou, X.L., and Cheng, H.-M. (2018). Chemical vapor deposition growth and applications of two-dimensional materials and their heterostructures. *Chemical Reviews* 118 (13): 6091–6133.

43 Wang, H., Chen, Y., Duchamp, M. et al. (2018). Large-area atomic layers of the charge-density-wave conductor $TiSe_2$. *Advanced Materials* 30 (8).

44 Hafeez, M., Gan, L., Li, H.Q. et al. (2016). Chemical vapor deposition synthesis of ultrathin hexagonal ReSe2 flakes for anisotropic raman property and optoelectronic application. *Advanced Materials* 28 (37): 8296–8301.

45 Wu, J.X., Tan, C.W., Tan, Z.J. et al. (2017). Controlled synthesis of high-mobility atomically thin bismuth oxyselenide crystals. *Nano Letters* 17 (5): 3021–3026.

46 Gao, T., Zhang, Q., Li, L. et al. (2018). 2D ternary chalcogenides. *Advanced Optical Materials* 6 (14): 1800058.

47 Tan, C.L. and Zhang, H. (2015). Epitaxial growth of hetero-nanostructures based on ultrathin two-dimensional nanosheets. *Journal of the American Chemical Society* 137 (38): 12162–12174.

48 van der Zande, A.M., Huang, P.Y., Chenet, D.A. et al. (2013). Grains and grain boundaries in highly crystalline monolayer molybdenum disulphide. *Nature Materials* 12 (6): 554–561.

49 Shi, Y.M., Li, H.N., and Li, L.-J. (2015). Recent advances in controlled synthesis of two-dimensional transition metal dichalcogenides via vapour deposition techniques. *Chemical Society Reviews* 44 (9): 2744–2756.

50 Gao, Y., Hong, Y.L., Yin, L.C. et al. (2017). Ultrafast growth of high-quality monolayer WSe_2 on Au. *Advanced Materials* 29 (29): 1700990.

51 Zhang, Z.W., Chen, P., Duan, X.D. et al. (2017). Robust epitaxial growth of two-dimensional heterostructures, multiheterostructures, and superlattices. *Science* 357 (6353): 788–792.

52 Liu, C., Xu, X.Z., Qiu, L. et al. (2019). Kinetic modulation of graphene growth by fluorine through spatially confined decomposition of metal fluorides. *Nature Chemistry* 11 (8): 730–736.

53 Kang, K., Xie, S.E., Huang, L.J. et al. (2015). High-mobility three-atom-thick semiconducting films with wafer-scale homogeneity. *Nature* 520 (7549): 656–660.

54 Chen, C., Chen, X.D., Wu, C.W. et al. (2022). Air-stable 2D Cr_5Te_8 nanosheets with thickness-tunable ferromagnetism. *Advanced Materials* 34 (2): 2107512.

55 Yan, C.Y., Gan, L., Zhou, X. et al. (2017). Space-confined chemical vapor deposition synthesis of ultrathin HfS2 flakes for optoelectronic application. *Advanced Functional Materials* 27 (39): 1702918.

56 Wang, Q., Shi, R., Zhao, Y.X. et al. (2021). Recent progress on kinetic control of chemical vapor deposition growth of high-quality wafer-scale transition metal dichalcogenides. *Nanoscale Advances* 3 (12): 3430–3440.

57 Dong, J.C., Zhang, L.N., Dai, X.Y., and Ding, F. (2020). The epitaxy of 2D materials growth. *Nature Communications* 11 (1): 5862.

58 Suenaga, K., Ji, H.G., Lin, Y.-C. et al. (2018). Surface-mediated aligned growth of monolayer MoS_2 and in-plane heterostructures with graphene on sapphire. *ACS Nano* 12 (10): 10032–10044.

59 Li, T.T., Guo, W., Ma, L. et al. (2021). Epitaxial growth of wafer-scale molybdenum disulfide semiconductor single crystals on sapphire. *Nature Nanotechnology* 16 (11): 1201–1207.

60 Yang, P.F., Liu, F.C., Li, X. et al. (2023). Highly reproducible epitaxial growth of wafer-scale single-crystal monolayer MoS_2 on sapphire. *Small Methods* 19: 2300165.

61 Ma, Z.P., Wang, S.Y., Deng, Q.X. et al. (2020). Epitaxial growth of rectangle shape MoS_2 with highly aligned orientation on twofold symmetry a-plane sapphire. *Small* 16 (16): 2000596.

62 Bian, R.J., Li, C.C., Liu, Q. et al. (2022). Recent progress in the synthesis of novel two-dimensional van der Waals materials. *National Science Review* 9 (5), nwab164.

63 Chen, T.A., Chuu, C.P., Tseng, C.C. et al. (2020). Wafer-scale single-crystal hexagonal boron nitride monolayers on Cu (111). *Nature* 579 (7798): 219–223.

64 Wang, L., Xu, X.Z., Zhang, L.N. et al. (2019). Epitaxial growth of a 100-square-centimetre single-crystal hexagonal boron nitride monolayer on copper. *Nature* 570 (7759): 91–95.

65 Xu, X.L., Pan, Y., Liu, S. et al. (2021). Seeded 2D epitaxy of large-area single-crystal films of the van der Waals semiconductor 2H $MoTe_2$. *Science* 372 (6538): 195–200.

66 Cheng, R., Jiang, S., Chen, Y. et al. (2014). Few-layer molybdenum disulfide transistors and circuits for high-speed flexible electronics. *Nature Communications* 5: 5143.

67 Li, S.L., Wakabayashi, K., Xu, Y. et al. (2013). Thickness-dependent interfacial coulomb scattering in atomically thin field-effect transistors. *Nano Letters* 13 (8): 3546–3552.

68 Liu, Y.C. and Gu, F.X. (2021). A wafer-scale synthesis of monolayer MoS_2 and their field-effect transistors toward practical applications. *Nanoscale Advances* 3 (8): 2117–2138.

69 Kim, S., Konar, A., Hwang, W.S. et al. (2012). High-mobility and low-power thin-film transistors based on multilayer MoS_2 crystals. *Nature Communications* 3: 1011.

70 Yan, J., Xia, J., Wang, X. et al. (2015). Stacking-dependent interlayer coupling in trilayer MoS_2 with broken inversion symmetry. *Nano Letters* 15 (12): 8155–8161.

71 Zhang, X.M., Nan, H.Y., Xiao, S.Q. et al. (2019). Transition metal dichalcogenides bilayer single crystals by reverse-flow chemical vapor epitaxy. *Nature Communications* 10 (1): 598.

72 Han, A., Aljarb, A., Liu, S. et al. (2019). Growth of 2H stacked WSe_2 bilayers on sapphire. *Nanoscale Horizons* 4 (6): 1434–1442.

73 Li, J.W., Wang, S.P., Li, L. et al. (2022). Chemical vapor deposition of 4 inch wafer-scale monolayer $MoSe_2$. *Small Science* 2 (11): 2200062.

74 Wang, Q.Q., Tang, J., Li, X.M. et al. (2022). Layer-by-layer epitaxy of multi-layer MoS_2 wafers. *National Science Review* 9 (6), nwac077.

75 Li, X.F., Zhang, Z.F., Gao, T.T. et al. (2022). Van der Waals epitaxial trilayer MoS_2 crystals for high-speed electronics. *Advanced Functional Materials* 32 (46): 2208091.

76 Liu, L., Li, T.T., Ma, L. et al. (2022). Uniform nucleation and epitaxy of bilayer molybdenum disulfide on sapphire. *Nature* 605 (7908): 69–75.

77 Ma, W., Chen, M.L., Yin, L.C. et al. (2019). Interlayer epitaxy of wafer-scale high-quality uniform AB-stacked bilayer graphene films on liquid Pt_3Si/solid Pt. *Nature Communications* 10 (1): 2809.

78 Zhang, Z.B., Ding, M.C., Cheng, T. et al. (2022). Continuous epitaxy of single-crystal graphite films by isothermal carbon diffusion through nickel. *Nature Nanotechnology* 17 (12): 1258–1264.

79 Ma, K.Y., Zhang, L., Jin, S. et al. (2022). Epitaxial single-crystal hexagonal boron nitride multilayers on Ni (111). *Nature* 606 (7912): 88–93.

80 Li, W.B., Qian, X.F., and Li, J. (2021). Phase transitions in 2D materials. *Nature Reviews Materials* 6 (9): 829–846.

81 Park, J.C., Yun, S.J., Kim, H. et al. (2015). Phase-engineered synthesis of centimeter-scale 1T′- and 2H-molybdenum ditelluride thin films. *ACS Nano* 9 (6): 6548–6554.

82 Qian, X.f., Liu, J.w., Fu, L., and Li, J. (2014). Quantum spin Hall effect in two-dimensional transition metal dichalcogenides. *Science* 346 (6215): 1344–1347.

83 Keum, D.H., Cho, S., Kim, J.H. et al. (2015). Bandgap opening in few-layered monoclinic $MoTe_2$. *Nature Physics* 11 (6): 482–486.

84 Kang, L.X., Ye, C., Zhao, X.X. et al. (2020). Phase-controllable growth of ultra-thin 2D magnetic FeTe crystals. *Nature Communications* 11 (1): 3729.

85 Zhang, S.C., Wu, Y., Gao, F. et al. (2022). Field effect transistor sensors based on in-plane 1T′/2H/1T′ $MoTe_2$ heterophases with superior sensitivity and output signals. *Advanced Functional Materials* 32 (41): 2205299.

86 Tang, L., Tan, J.Y., Nong, H.Y. et al. (2020). Chemical vapor deposition growth of two-dimensional compound materials: controllability, material quality, and growth mechanism. *Accounts of Materials Research* 2 (1): 36–47.

87 Liu, L., Wu, J.X., Wu, L.Y. et al. (2018). Phase-selective synthesis of 1T' MoS_2 monolayers and heterophase bilayers. *Nature Materials* 17 (12): 1108–1114.

88 Deng, Q.X., Li, X.B., Si, H.Y. et al. (2020). Strong band bowing effects and distinctive optoelectronic properties of 2H and 1T′ phase-tunable $MoxRe_1–xS_2$ Alloys. *Advanced Functional Materials* 30 (34): 2003264.

89 Han, W., Zheng, X.D., Yang, K. et al. (2023). Phase-controllable large-area two-dimensional In_2Se_3 and ferroelectric heterophase junction. *Nature Nanotechnology* 18 (1): 55–63.